Available online at www.sciencedirect.com
ScienceDirect
Catalysis Today 133–135 (2008) 142–148
CATALYSIS TODAY
www.elsevier.com/locate/cattod

Dry reforming of CH_4 over solid solutions of $LaNi_{1-x}Co_xO_3$

Gustavo Valderrama [a,*], A. Kiennemann [b], M.R. Goldwasser [c]

[a] *Laboratorio de Catálisis, Petróleo y Petroquímica, Unidad de Estudios Básicos, Universidad de Oriente - Núcleo Bolívar, La Sabanita, Calle San Simón, Estado Bolívar 8001, Venezuela*

[b] *Laboratoire des Matériaux, Surfaces et Procédés pour la Catalyse, UMR 7515, ECPM, Université Louis Pasteur, 25 rue Becquerel, 67087 Strasbourg Cedex 2, France*

[c] *Centro de Catálisis Petróleo y Petroquímica, Facultad de Ciencias, Universidad Central de Venezuela, Los Chaguaramos Paseo Ilustre, Caracas 1040, Venezuela*

Available online 1 February 2008

Abstract

$LaNi_{1-x}Co_xO_3$ perovskite-type oxides were synthesized by the sol–gel resin method and used as catalysts precursors in the dry reforming of methane to syngas between 600 and 800 °C at atmospheric pressure, the reaction was studied under continuous flow using an mixture of CH_4:CO_2 = 1:1. The solids were characterized by X-ray diffraction (XRD), BET specific surface area and temperature-programmed reduction (TPR).

XRD analysis of the solids shows $LaNiO_3$ and/or $LaCoO_3$ as the main phases present on the solids depending on the degree of substitution. The more intense peaks and cell parameters showed formation of Ni-Co solid solutions. The as-synthesized solids were reduce during catalytic tests to form Ni^0, Co^0 and $La_2O_2CO_3$ as the active phases which remain during the reaction and are responsible for the high activity shown by the solids inhibiting carbon formation, with CH_4 and CO_2 equilibrium conversions near 100%, except for $LaCoO_3$ that showed a poor activity.
© 2008 Elsevier B.V. All rights reserved.

Keywords: Resin method; (Ni, Co)-solid solutions; (Ni, Co)-perovskites; Dry reforming of methane; Syngas production; Catalytic activity; Carbon deposition

1. Introduction

In the beginnings of the third millennium, the natural gas is glimpsed as the fuel of the future, due to the world wide considerable proven reserves and to the strong dependence of the increasing petroleum demands [1]. Recognition of this situation has produced a growing interest in the development of new technologies to efficiently transform natural gas prevailing study of the dry reforming of CH_4 (Eq. (1)) that produce syngas (i.e. $CO + H_2$) with $H_2/CO \leq 1$ ratio, favourable for Fischer–Tropsch reactions to produce liquid fuels [2] also contributes to minimize of emissions from these gases to the environment [3].

$$CH_4 + CO_2 = 2CO + 2H_2 \quad \Delta H_{298} = 247\,\text{kJ/mol} \qquad (1)$$

One disadvantage of this reaction is the accumulation of carbon by methane cracking or CO disproportion over surface catalytic, which requires catalytic systems that inhibits carbon formation. Condition that promotes the development of new active and resistant to coke catalysts, an alternative is the use of Ni catalysts, very well known in steam reforming [4], due to the kindness that this metal offers its interesting redox properties and relatively lower cost that makes it easily accessible.

In this sense, an increasing interest exists in the synthesis of Ni-based catalysts or precursors resistant to coke formation, introducing the Ni in perovskite-type structure (ABO_3), which are well-defined structures that produces very small highly dispersed metallic particles, in the order of the nanometers, after reduction processes, promoting activity and stability and suppressing coke formation [5]. Another advantage of perovskite-type structures is the possibility of total or partial substitution of its cations modifying their oxidation state, the mobility of oxygen lattice and the redox properties [6] that modify the catalytic activity and stability. The paper shows the results obtained during the dry reforming of methane over $LaNi_{1-x}Co_xO_3$ ternary perovskites-type precursor's materials, to prevent coke formation, also includes the special XRD analyses and the behaviour under reducing atmosphere of the solids (TPR).

* Corresponding author.
E-mail address: vgustavo@udo.edu.ve (G. Valderrama).

0920-5861/$ – see front matter © 2008 Elsevier B.V. All rights reserved.
doi:10.1016/j.cattod.2007.12.069

2. Experimental

2.1. Synthesis of perovskite-type oxides

$LaNi_{1-x}Co_xO_3$ ternary oxides were prepared by the resin sol–gel method [7], dissolving the expected stoichiometric amounts of cations acetate in excess propionic acid. Solutions of metals B (Ni and/or Co) were mixed and lanthanum solution was then added. The resulting solution was refluxed at a temperature close to the boiling point of the propionic acid until total evaporation to form a resin. Then liquid N_2 is added to crystallize the resin that is dried overnight at 110 °C and calcined at 750 °C (4 h, 3 °C/min).

2.2. Characterization

The solids were characterized before and after the catalytic test by techniques such as X-ray diffraction (XRD), BET specific surface area and temperature-programmed reduction (TPR).

XRD analyses were performed to determined the internal structure of the synthesized solids, using a SIEMENS D5000 equipment with a copper anode ($K\alpha_{Cu}$ = 1.54056 Å), operated an accelerating voltage of 40 kV and intensity of 20 mA. The acquisition of the diffraction data depends on the required study; e.g. the diffractograms were recorded in the angular zone between θ and 2θ values 10°–90° with a step size of 0.05 and 27 s per step to obtained initials phases and calculation the cell parameters, a step size of 0.02 and 1 s per step after RTP and catalytic test, and values range 32°–35° with a step size of 0.02 and 30 s per step to confirm the solid solution formation. The powder camera method that consists on the pulverization of the solid was used to guarantee a homogeneous and abundant size of grains that promotes the formation of all the symmetry planes increasing the sensibility of each sign. Phase's recognition was obtained by comparison with JCPDS files using the database PDF and software EVA 3.30 programs.

BET specific surface areas were determined by N_2 adsorption at 77 K, using ~100 mg of previously out gassed sample a 10^{-6} Torr with Sortometer Coulter SA 3100 equipment.

TPR analyses were carried out in a quartz reactor using 50 mg of sample, under reducing mixture flow of H_2 (2 ml/min) diluted in argon (50 ml/min) and increasing from room temperature to 900 °C at 15 °C/min. The coke deposition on the catalysts after reaction was determined by this technique with similar procedure. The calibration of hydrogen uptake was done by referring to the TPR peak of known amount of a standard (pure H_2) taken in identical conditions.

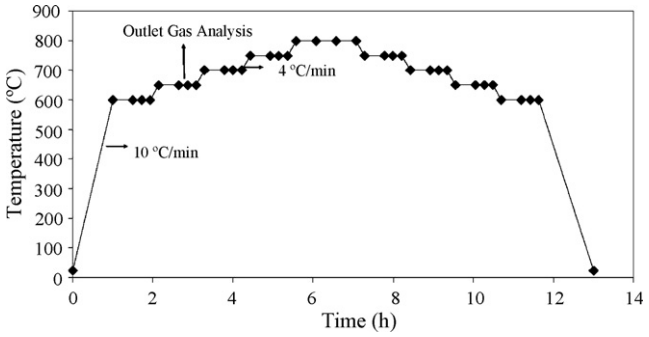

Fig. 1. Thermal treatment used in the dry reforming of CH_4.

2.3. Dry reforming of methane

Catalytic studies were carried out, in a 6.6 mm i.d. quartz reactor with ~200 mg of solid without previous reduction, between 600 and 800 °C at atmospheric pressure, under a fixed-bed continuous flow (CH_4:CO_2 = 1:1 ratio, Ar as diluents 35 ml/min and N_2 as internal standard 5 ml/min and total flow of 50 ml/min, WHSV = 15 l/h g) The outlet gas was analysed simultaneously by two gas chromatographs, the first allows separating hydrogen, nitrogen, methane and monoxide of carbon on a Tami 5 column; the second quantified argon, methane and CO_2 on a Hayesep R column.

Two temperature regimes for dry reforming of methane were used. The first one temperature was increased from room temperature to 600 °C at a rate of 10 °C/min. Once steady state conditions were reached (~30 min) analyses started and continue within 15 min intervals (Fig. 1). The temperature was then increased with 50 °C intervals from 600 to 800 °C at 4 °C/min, following a similar procedure ''Semi-cycle''. A reverse protocol was followed to decrease the temperature from 800 to 600 °C ''cycle''. During the cycle, methane and CO_2 conversions and H_2 and CO selectivities were calculated in a similar way as reported elsewhere [8].

3. Results and discussions

The results of BET specific surface area, XRD, reduction percentages and carbon formation are summarized in the Table 1. It is observed that the sol–gel method via propionic

Table 1
BET specific surface area and, XRD results of the synthesized solids at 750 °C

Precursor solid	SA (m^2/g)	XRD initial phase	XRD after redox	XRD after reaction
$LaNiO_3$	7.5	$LaNiO_3$	Ni, La_2O_3	Ni, $La_2O_2CO_3$
$LaNi_{0.8}Co_{0.2}O_3$	6.9	$LaNiO_3$	Ni, Co, La_2O_3	Ni, Co, $La_2O_2CO_3$
$LaNi_{0.7}Co_{0.3}O_3$	39.4	$LaNiO_3$	Ni, Co, La_2O_3	Ni, Co, $La_2O_2CO_3$
$LaNi_{0.5}Co_{0.5}O_3$	9.5	$LaNiO_3$, $LaCoO_3$	Ni, Co, La_2O_3	Ni, Co, $La_2O_2CO_3$
$LaNi_{0.4}Co_{0.6}O_3$	5.6	$LaCoO_3$	Ni, Co, $La(OH)_3$	Ni, Co, $La_2O_2CO_3$
$LaNi_{0.2}Co_{0.8}O_3$	6.4	$LaCoO_3$	Ni, Co, La_2O_3	Ni, Co, $La_2O_2CO_3$
$LaCoO_3$	4.2	$LaCoO_3$	Co, La_2O_3	Co, La_2O_3

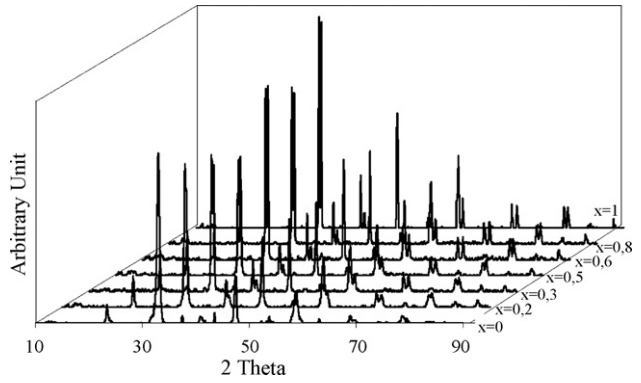

Fig. 2. XRD patterns of $LaNi_{1-x}Co_xO_3$ system.

acid is appropriate for the synthesis of crystalline phases of perovskite-type oxides in the expected stoichiometric with specific surface areas in the range of 4–39 m^2/g, in agreements with previously reported values [5,8].

The diffraction patterns of the as-synthesized solids (Fig. 2), showed a good crystallization of the perovskite phase without the presence of polluting phases. Which was dependent on the substitution degree (x): for $x \leq 0.4$ isomorphs $LaNiO_3$ solids are obtained, while for $x \geq 0.6$ $LaCoO_3$ structure is formed (Table 1), in agreement with previously reported observations [9].

Amplification of the angular area between 32° and 35° corresponding to $LaNi_{1-x}Co_xO_3$ more intense peaks diffraction (Fig. 3), shows a split characteristic of rhombohedra symmetry [10]. Although $LaNiO_3$ main peak does not show this splitting its distortion is rhombohedra, since the second peak with a very weak signal is overlap giving to an asymmetric wide peak [11] (Fig. 3). While the position of the peaks of maximum intensity of ternary solids shift regularly between the peaks used as reference for $LaNiO_3$ (33.16°) and $LaCoO_3$ (33.44°) binary perovskite-type oxides, these signals progressive shift with increasing Co content (Fig. 3) suggesting the formation of a solid solution [12].

To investigate the effect on rhombohedra cell parameters of the partial substitution of B cation, these parameters were calculated for each x value, indexing the two most intensive diffraction peaks (Fig. 2) in the planes corresponding to (1 1 0) and (2 0 2) $LaNiO_3$ (JCPDS 33-0711) to an ideal hexagonal system, which were used the rhombohedra parameters obtain (Table 2). Hexagonal and rhombohedra symmetry was calculated through the equations reported by Klug and Alexander [13].

Table 2
Lattice parameters for hexagonal and rhombohedra symmetries

$LaNi_{1-x}Co_xO_3$ (x)	Hexagonal symmetry			Rhombohedra symmetry	
	a (Å)	b (Å)	c (Å)	a (Å)	α
0	5.4327	5.4327	13.2210	5.4091	60.29
0.2	5.4287	5.4287	13.2218	5.4080	60.25
0.3	5.4296	5.4296	13.1608	5.3919	60.47
0.5	5.4327	5.4327	13.1304	5.3846	60.59
0.6	5.4121	5.4121	13.1468	5.3821	60.37
0.8	5.4308	5.4308	13.1178	5.3798	60.60
1.0	5.4175	5.4175	13.0927	5.3693	60.60

The cell rhombohedra parameters of $LaNi_{1-x}Co_xO_3$ decreases with Co content (Fig. 4) from 5.409 to 5.369 Å, since the substitution of the cation Ni^{3+} with a 0.56 Å radium for Co^{3+} with a 0.52 Å radium causes a decrease of the distance $d_{B\text{-}O}$ in the perovskite structure. The calculated rhombohedra cell parameters (Table 2) follow Vegart Law [14] that defines solid solutions, that is to say, they show a lineal variation with respect to the substitution degree (Fig. 4), confirming the solid solutions formation among these ternary systems. The lineal variation serves as a calibration method of lattice parameters, to evaluate the migration of Ni or Co of perovskite-type structure that are not completely destroyed or that could be formed during the catalytic evaluation, without knowing the exact deformation of the formed structure.

Analysis of the reduction profiles of these solids (Fig. 5) shows the several peaks formations, which correspond to different Ni and Co intermediate species. For example, during the reduction of $LaNiO_3$; the XRD patterns of first α-peak at 360 °C (Fig. 6), show that $LaNiO_{2.7}$ is formed without total destruction of the perovskite-type structure, tolerating a significant oxygen deficiency similar to the oxygen desorption and surface reduction 19.1% (Table 3), demonstrating the mobility of lattice oxygen [15]. The second peak appears at 395 °C corresponding to $La_2Ni_2O_5$ phase, and the third larger

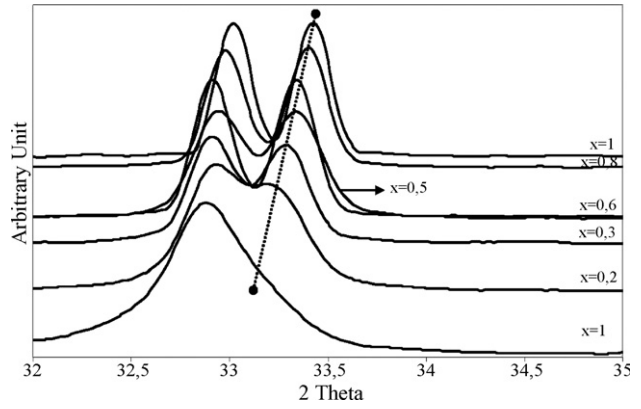

Fig. 3. XRD patterns of $LaNi_{1-x}Co_xO_3$ more intense peaks.

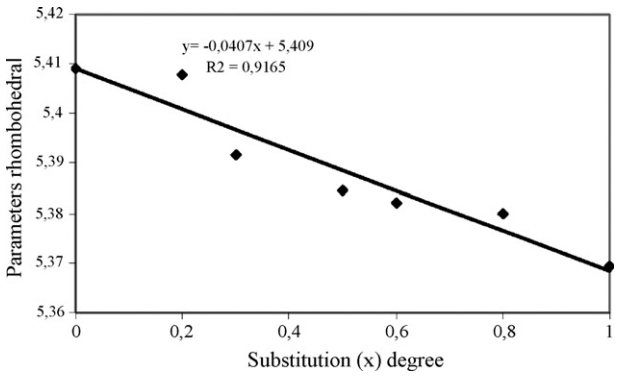

Fig. 4. The rhombohedra a_R cell parameters.

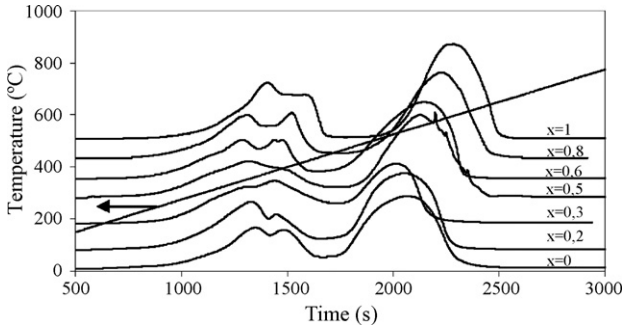

Fig. 5. $LaNi_{1-x}Co_xO_3$ TPR profile.

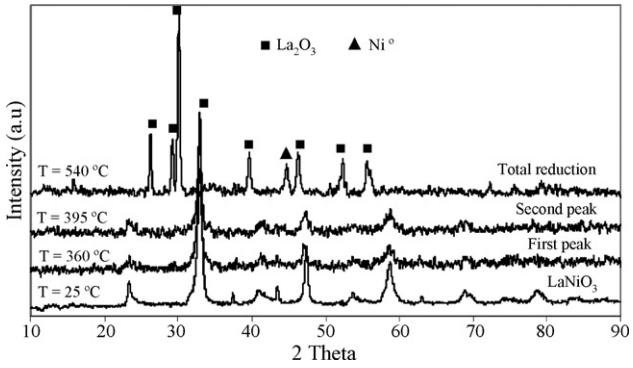

Fig. 6. $LaNiO_3$ crystalline phases as a function of the reduction temperature.

β-peak at 540 °C bulk reduction correspond to Ni^0 and La_2O_3 occurs [16]. Based on these results, the reduction steps are written as follows:

$$2LaNiO_3 + H_2 \rightarrow La_2Ni_2O_5 + H_2O \quad (2)$$

$$La_2Ni_2O_5 + 2H_2 \rightarrow La_2O_3 + 2Ni + 2H_2O \quad (3)$$

While, the diffraction patterns of different peaks $LaCoO_3$ (Fig. 7), show that at 377 °C the reduction occurs very quickly hindering identification of the possible phases formed (Fig. 7). However, it has been reported [17] that at 385 °C the $LaCoO_{2.75}$ phase is obtained. Based on this result we assume that the first reduction α-peak corresponds to this phase with reduction 25.3% (Table 3), similar behaviour to $LaNiO_3$, which at 420 °C decreases to form $La_4Co_3O_{10}$ without total destruction of the $LaCoO_3$ phase corroborating the mobility of oxide ions, then at 600 °C the total reduction with the formation of Co^0 and La_2O_3

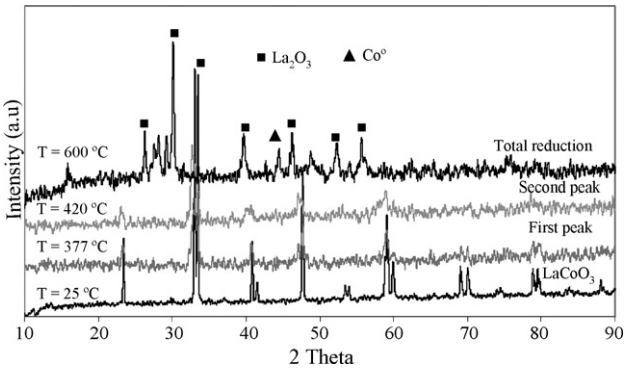

Fig. 7. $LaCoO_3$ crystalline phases as a function of the reduction temperature.

occurs (Fig. 7). According to:

$$LaCoO_3 + 0.25H_2 \rightarrow LaCoO_{2.75} + 0.25H_2O \quad (4)$$

$$4LaCoO_{2.75} + H_2 \rightarrow La_4Co_3O_{10} + Co + H_2O \quad (5)$$

$$La_4Co_3O_{10} + 4H_2 \rightarrow 2La_2O_3 + 3Co + 4H_2O \quad (6)$$

The reduction of the solid $LaNi_{0.5}Co_{0.5}O_3$ follows the same scheme observed for the perovskite-type oxide used as reference (Eqs. (2)–(6)), behaviour that can be extrapolated to all the ternary solids.

When comparing the reduction temperatures of these binary oxides to other synthesis methods reported [8,16,18] with similar surfaces areas, it is observed that propionic acid synthesis method favours reduction of the solids at lower temperatures. It is noted that Ni- or Co-substitute oxide begins to reduce at lower temperature than the host oxide (Table 3) even when the host and substitute cations have the same valence, this synergetic effect important should be considered during catalytic test.

The XRD patterns do not show Ni^0-Co^0 alloy formation suggesting a high metallic dispersion. However, alloy formation can not be discarded between metals with particles size ≤10 Å, below the detection limit of X-rays [19] since peaks of Ni^0 and Co^0 phases from ternary solids (Fig. 8) are among those of binary perovskites.

$LaNi_{1-x}Co_xO_3$ precursor was used without reduction prior to catalytic measurements. Changes in CO yield as a function of temperature are shown in Fig. 9. It is observed that an increase in Co content on the precursor perovskite-type oxide rises the initial temperature at which the reforming reaction takes place,

Table 3
Temperatures, reduction and coke results of the synthesized solids at 750 °C

Precursor solid	1st Peak		2nd Peak		3rd Peak		Total	
	T (°C)	Red (%)	T (°C)	Red (%)	T (°C)	Red (%)	Red (%)	Coke (%)
$LaNiO_3$	360	19.1	395	12.5	540	54.3	85.9	0.7
$LaNi_{0.8}Co_{0.2}O_3$	355	23.5	385	10.2	537	50.2	83.9	2.8
$LaNi_{0.7}Co_{0.3}O_3$	347	20.8	385	26.9	530	38.7	86.4	0.9
$LaNi_{0.5}Co_{0.5}O_3$	353	22.8	390	10.7	556	55.1	88.6	2.7
$LaNi_{0.4}Co_{0.6}O_3$	348	19.8	390	13.4	562	57.3	90.5	0.1
$LaNi_{0.2}Co_{0.8}O_3$	356	21.2	408	12.7	586	52.5	86.4	0.3
$LaCoO_3$	377	25.3	420	14.6	600	57.1	97.0	0.3

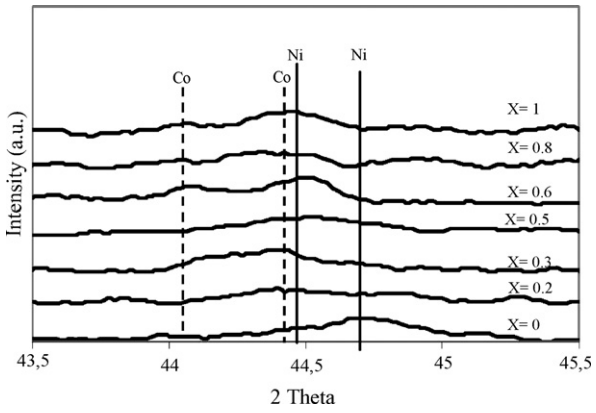

Fig. 8. XRD patterns of peaks respect to Ni^0 and Co^0 phases of $LaNi_{1-x}Co_xO_3$.

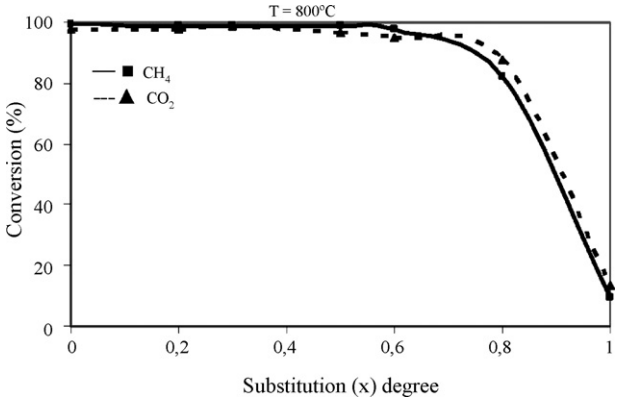

Fig. 10. CH_4 and CO_2 conversions on unreduced $LaNi_{1-x}Co_xO_3$ at 800 °C.

due to the fact that Co reduction to Co^0 requires higher temperatures than Ni (Table 3).

The observed difference in CO yield during the rise and decrease of temperature (Fig. 9) is known as hysteresis phenomenon [20], which occurs due to the initial lack of activity of the solids at 650 °C, produced by the absence of Co^0 active species. Such a phenomenon is not important for high Ni ($x \leq 0.3$) contents reaching a stationary state of activation between 650 and 800 °C. It is evident that activation of the solids occurs in situ, due to the presence of a reducing atmosphere formed by the gases (CH_4, CO, H_2) in the reaction media that promotes formation of the active species Ni^0, Co^0 and $La_2O_2CO_3$ (Table 1).

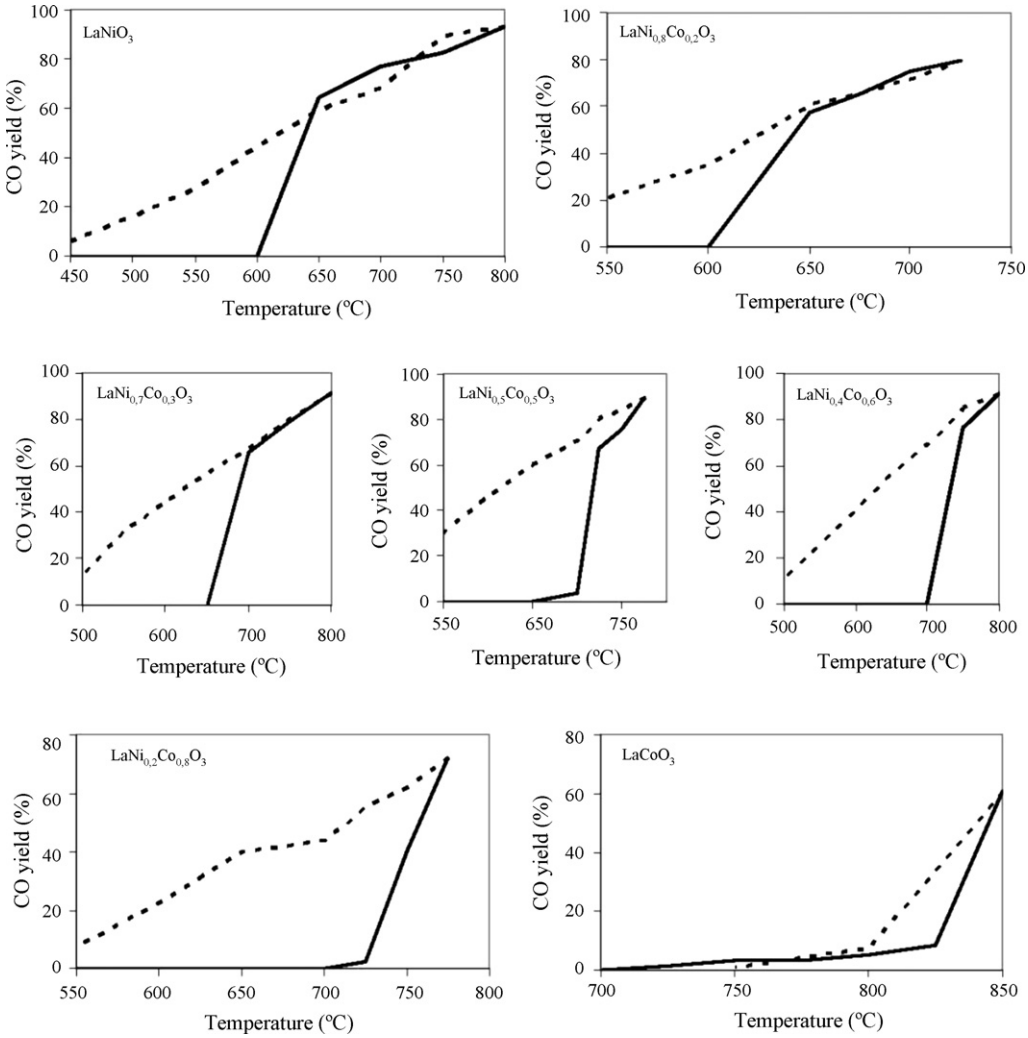

Fig. 9. CO yield as a function of temperature. Rise (—) and descent (- - -) cycles.

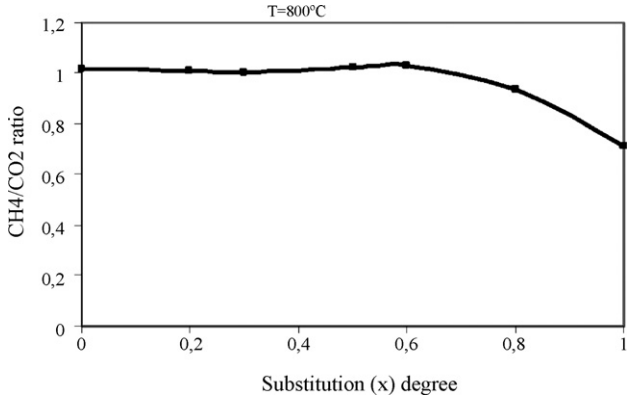

Fig. 11. Dry reforming of methane: X_{CH_4}/X_{CO_2} ratio.

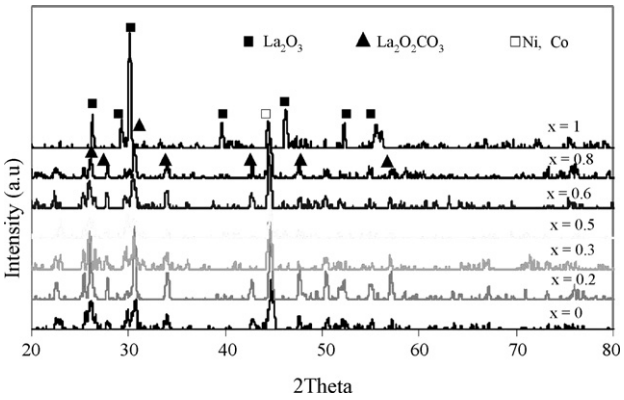

Fig. 13. XRD patterns of after-reaction $LaNi_{1-x}Co_xO_3$.

The evolution of CH_4 and CO_2 conversions during the dry reforming of methane at 800 °C over the solids solution synthesized is shown in Fig. 10. It is observed that conversions of both gases are favoured on the Ni ($x \leq 0.6$) rich solids, with values close to the thermodynamic balance (~100%) and a X_{CH_4}/X_{CO_2} ratio close to 1 (Fig. 11), suggesting that Ni favours reaction (1).

$LaCoO_3$ showed a poor activity (Fig. 9) due to the initial activation time needed to in situ reduce Co^{3+} to Co^0 [21] and to the absence of $La_2O_2CO_3$ phase (Table 1). However, synergetic effect have also been observed in $LaNi_{0.2}Co_{0.8}O_3$ with the presence of Ni in doping quantities since presents high activity for the reaction (Fig. 9) reaching CH_4 and CO_2 conversions of 82 and 88%, respectively, which indicated that the presence of Ni promotes Co activation and eliminates the initial induction period.

On the other hand, it is observed (Fig. 12) that the Ni ($x \leq 0.6$) rich solids produce high selectivities toward the formation of syngas, with CH_4 conversions slightly higher than that of CO_2 and H_2 selectivities slightly superior to that of CO (Fig. 9). This indicates that the reactions (7) and (8) are occurring in a very small extension:

$$CH_4 = C + 2H_2 \quad \Delta H_{298} = 74.85\,\text{kJ/mol} \tag{7}$$

$$CO + H_2O = CO_2 + H_2 \quad \Delta H_{298} = -41.17\,\text{kJ/mol} \tag{8}$$

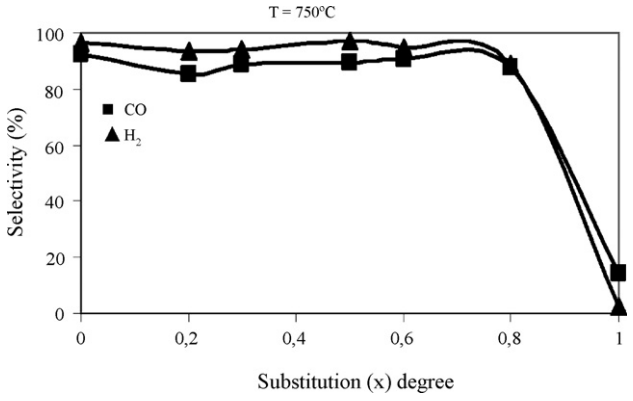

Fig. 12. CO and H_2 selectivities obtained for $LaNi_{1-x}Co_xO_3$.

Accordingly, the methane decomposition reaction (7) increases CH_4 conversion and H_2 selectivity. While water gas shifts reaction (8) decreases the selectivity to CO and increases H_2 selectivity.

XRD analyses of after-reaction solids reveal the presence of $La_2O_2CO_3$, Ni and Co phases (Fig. 13) and of very small quantities of coke determined by TPR (Table 3). The high dispersion of the metallic phases, the presence of $La_2O_2CO_3$ that plays a very important paper in the reforming (Eq. (9)) and reacts with methane and regenerate La_2O_3 inhibits coke deposits and is responsible for the high activities shown by these solid solutions.

$$La_2O_3 + CO_2 \rightarrow La_2O_2CO_3 + CH_4 \rightarrow La_2O_3 + 2CO + 2H_2 \tag{9}$$

It is important to point out that in spite of the severe reaction conditions used (Fig. 1), only small quantities of coke was formed (Table 3), indicating that interaction between metallic species Ni^0-Co^0 cause an synergetic effect, no clearly understood, that play a very important role in the catalytic behaviour. Therefore, we propose that doping quantities of Co, which reduces at higher temperatures (Fig. 5), stabilize the particles of metallic Ni inhibiting coke formation, while doping quantities of Ni diminishes the temperature of reduction of Co (Fig. 5) accelerating the activation of the solid.

4. Conclusions

The resin sol–gel method via propionic acid is appropriate for the synthesis of solid solutions of perovskite-type structure with high degree of purity. The formation of Ni^0 and Co^0 active species occurs at low temperatures through intermediate species formed by stepwise reduction.

The dry reforming of methane shows that the precursor $LaNi_{1-x}Co_xO_3$ ($x \leq 0.8$) produce very active catalysts for this reaction, with conversions and selectivities close to thermodynamic equilibrium (~100%). This activity is attributed to the in situ formation of Ni^0-Co^0 particles highly dispersed on $La_2O_2CO_3$ matrix that inhibits coke formation in spite of the severe reaction conditions.

Interactions between the metallic phases Ni^0-Co^0 originate synergetic effects that contribute to the stabilization of the catalyst increasing the time of useful life. Doping quantities of Co stabilize Ni^0 particles suppressing coke formation, while the presence of small quantities of Ni favours reduction of the Co accelerating the activation of the solid.

Acknowledgements

The authors are grateful to Venezuela FONACIT for its financial support through Projects Petroleum Agenda No. 97-003739, PICS PI 2003000024 and CI-UDO-Bolívar, as well as, Fundacite-Guayana.

References

[1] BP Statistical Review of World Energy, Londres Inglaterra: BP Junio, 2003, 20.
[2] J.R. Ross, A.N. van Keulen, M.E. Hegarty, K. Seshan, Catal. Today 30 (1996) 193.
[3] Noticias BBC MUNDO.com. 2005, http://news.bbc.co.uk/hi/spanish/specials/2005/kioto/newsid_4234000/4234085.stm#xq1.
[4] J.R. Rostrup-Nielsen, J.-H. Bak Hansen, J. Catal. 144 (1993) 39.
[5] M.R. Goldwasser, M.E. Rivas, E. Pietri, M.J. Pérez-Zurita, M.L. Cubeiro, Grivobal-Constant, G. Leclercq, J. Mol. Catal. A 228 (2005) 325.
[6] M.A. Peña, J.L.G. Fierro, Chem. Rev. 101 (2001) 1981.
[7] J.L. Rehspringer, J.C. Bernier, Mater. Res. Soc. Symp. Proc. 72 (1986) 67.
[8] G. Valderrama, M.R. Goldwasser, C. Urbina de Navarro, J.M. Tatibouët, J. Barrault, C. Batiot-Dupeyrat, F. Martinez, Catal. Today 107/108 (2005) 785.
[9] L. Bedel, A.C. Roger, C. Estournes, A. Kiennemann, Catal. Today 85 (2–4) (2003) 207.
[10] P. Lacorre, J.B. Torrance, J. Pannetier, A.I. Nazzal, P.W. Wang, T.C. Huang, J. Solid State Chem. 91 (1991) 225.
[11] H. Provendier, Tesis Doctoral en Química, Universidad Louis Pasteur, 1999, p. 65.
[12] J.S. Choi, K.I. Moon, Y.G. Kim, J.S. Lee, C.H. Kim, D. Trimm, Catal. Lett. 52 (1998) 163.
[13] H.P. Klug, L.E. Alexander, X-Ray Diffraction Procedure for Polycristalline and Amorphous Materials, second ed., Wiley, New York, 1974 .
[14] M. Stojanovic, R.G. Haverkamp, C.A. Mims, H. Moudallal, A. Jacobson, J. Catal. 165 (1997) 315.
[15] W.P. Finlandés, Solid State Ionics 129 (2000) 145.
[16] F. Martínez, C. Batiot-Dupeyrat, G. Valderrama, J. Tatibouët, Comptes Rendus Acad. Sci. Paris Serie IIc Chimie 4 (2001) 49.
[17] L.B. Sis, G.P. Wirtz, S.C. Sorenson, J. Appl. Phys. 44 (1973) 5553.
[18] C. Batiot-Dupeyrat, G. Valderrama, A. Meneses, F. Martínez, J. Barrault, J. Tatibouët, Appl. Catal. A 248 (2003) 143.
[19] C. Giacovazzo, Fundamentals of Cristallography, Oxford University Press, Oxford, RU, 1995.
[20] D. Dissanayake, M. Rosynek, K. Kharas, J. Catal. 132 (1991) 117.
[21] M.R. Goldwasser, M.E. Rivas, M.L. Lugo, E. Pietri, M.J. Pérez-Zurita, M.L. Cubeiro, A. Griboval-Constant, G. Leclercq, Catal. Today 107–108 (2005) 436.